Supplementary information

Room-temperature $FeSi_2$-doped Cu_2Se thermoelectric films with enhanced figure of merit

Masahiro Goto[1,*], Michiko Sasaki[1,*], Taku Moronaga[2], Toru Hara[3], and Yibin Xu[4]

[1]Thermal Energy Materials Group, Research Center for Materials Nanoarchitectonics (MANA), National Institute for Materials Science (NIMS), 1-2-1 Sengen, Tsukuba, Ibaraki 305-0047, Japan

[2]Electron Microscopy Unit, Materials Fabrication and Analysis Platform, Japan Research Network and Facility Services Division, National Institute for Materials Science (NIMS), 1-2-1 Sengen, Tsukuba, Ibaraki 305-0047, Japan

[3]Microstructure Analysis Group, Research Center for Structural Materials, National Institute for Materials Science (NIMS), 1-2-1 Sengen, Tsukuba, Ibaraki 305-0047, Japan

[4]Data-driven Inorganic Materials Group, Center for Basic Research on Materials, National Institute for Materials Science (NIMS), 1-2-1 Sengen, Tsukuba, Ibaraki 305-0047, Japan

*goto.masahiro@nims.go.jp; sasaki.michiko@nims.go.jp

Combinatorial Sputter Coating System (COSCOS)

A schematic of the combinatorial sputter coating system (COSCOS) is shown in Fig. S1. This system is a materials synthesis apparatus designed for integrated research and development, enabling efficient material exploration and device fabrication to discover high-performance materials and facilitating their practical application within a short timeframe. The system features a large hatch at the front of the main chamber, allowing for efficient loading and unloading of sample holders, typically accommodating 14 samples at once. The main chamber is evacuated using a high-capacity turbomolecular pump, achieving a vacuum level below 10^{-6} Pa without requiring a baking process. Because sample loading and unloading are unnecessary between coatings, contamination effects are minimized, and film property reproducibility is enhanced. During the coating process, the chamber pressure is monitored via a capacitance manometer. The system adjusts the gate valve's conductance to maintain a constant sputtering gas pressure through feedback control. The thermal conductivity between the individual sample holders and the multisample holder is suppressed using alumina spacers, ensuring that only the sample at the coating position is heated to approximately 1273 K by the heater. Meanwhile, the remaining 13 samples remain water-cooled, maintaining their temperatures below 353 K and preventing undesired thermal effects. Key coating parameters—including sputtering gas pressure, gas type and partial pressure, sputtering power, substrate temperature, substrate–target distance, and bias voltage—are fully adjustable and remotely controlled via an external control system. The shutter angle is also included as a coating parameter to enable trace element–doping by selectively exposing parts of the shutter coated with raw materials to the plasma. Sample preparation conditions are preregistered in a recipe, and once the recipe is initiated, the entire coating process is executed automatically. The film thickness, temperature, and gas pressure during deposition are monitored in real time, and the process is logged for easy identification of any abnormalities.

This approach has simplified the discovery of new materials—a task previously considered labor-intensive and often avoided—resulting in the development of materials that considerably enhance thermoelectric performance.

Scanning electron microscopy (SEM) and energy-dispersive X-ray spectroscopy (EDX) analyses

The surface morphologies of the $Cu_2Se_xSi_yFe_zO_t$ (CSSFO) thin films under different coating conditions—(a) 60 W, 298 K; (b) 60 W, 773 K; and (c) 120 W, 773 K—are shown in Fig. S4. The sample prepared at 60 W, 298 K exhibited a flat surface with noticeable cracks and precipitated particles. In contrast, the surfaces of the samples prepared at 60 W, 773 K and 120 W, 773 K were fully covered with tiny crystal grains. The elemental maps of the CSSFO films under these conditions are presented in Figs. S2 and S5. For the samples prepared at 60 W, 298 K, large particles containing O, Si, and Fe were observed (Fig. S5(a)). However, for the samples prepared at 60 W, 773 K and 120 W, 773 K, these large particles disappeared (Fig. S5(b) and S5(c)) and were replaced by numerous tiny FeO clusters (Fig. S2).

X-ray diffraction (XRD) analysis

The X-ray diffraction (XRD) spectra of the CSSFO samples under different coating conditions—(a) 60 W, 298 K; (b) 60 W, 773 K; (c) 80 W, 773 K; and (d) 100 W, 773 K—are shown in Fig. S6. Peaks corresponding to Cu_2Se, $Cu_{1.8}2Se$, and $Cu_{1.8}Se$ crystals were observed in all CSSFO samples. CuO peaks were identified in all samples coated at 773 K samples, while Cu_2O peaks appeared specifically in the samples prepared at 80 W, 773 K and 100 W, 773 K.

Electron backscatter diffraction (EBSD) analysis

An electron backscatter diffraction (EBSD) image of the CSSFO film coated at 120 W, 773 K is presented in Fig. S7. Band contrast and inverse pole figure map are shown in Fig. S7(a) and Fig. S7(b), respectively. The film contained various crystal structures with preferred crystal orientations that were intricately mixed. The crystal grain size was smaller near the substrate but grew larger toward the surface.

Surface-tetrahedron-like structure analysis

The X-ray photoelectron spectroscopy (XPS) depth profile of the CSSO film coated at 120 W, 773 K is shown in Fig. S8. The spectra include (a) Cu 2p, (b) O 1s, and (c) 3d peaks. These results clearly indicate a

Cu_2O peak along with very weak CuO peaks near the surface region. Furthermore, elemental mapping and electron diffraction of the tetrahedron-like structures on the sample surface were conducted. High-resolution transmission electron microscopy analysis showed that these structures were crystallized, and electron diffraction confirmed that they corresponded to Cu_2O crystals. These results are consistent with the XPS results.

Principal component analysis (PCA)

The XRD spectra, coating parameters (RF power and substrate temperature), and TE properties (electric conductivity, Seebeck coefficient, thermal conductivity, power factor, figure-of-merit (zT), and z were analyzed using principal component analysis (PCA). To further evaluate these data, the Lasso and random forest algorithms were employed, yielding R^2 values of 0.90 and 0.60, respectively. Given its higher accuracy, the Lasso analysis was selected. The corresponding heatmap is shown in Fig. S9.

The contribution of each principal component was 90% for PC1 and 9% for PC2, collectively accounting for the enter variance in the dataset. The components that were effective in increasing the zT value were PC1 and PC2, reducing both. In terms of the XRD peak behavior, decreases in PC1 and PC2 weakened the 002 peak intensity of Cu_2Se at ~13°, while the intensities of the 211 and 311 peaks (~25.5°) and 220 peak (~44°) were increased. Additionally, the intensities of the $Cu_{1.82}Se$ and $Cu_{1.8}Se$ peaks increased. Final analysis indicates that enhancing the growths of the Cu_2Se, $Cu_{1.82}Se$ and $Cu_{1.8}Se$ crystal phases plays a critical role in improving TE performance (zT value).

Temperature dependence of the figure of merit (zT)

A zT value of 0.69 was obtained at 298 K; however, estimating zT in the medium- to high-temperature range is important to understand the potential for expanding the range of applications. In general, the thermal conductivity of Cu_2Se decreases with the increase of temperature. Therefore, we estimated the zT value in the medium- to high-temperature range using the thermal conductivity at 298 K (Fig. S10). Consequently, a high zT value of 2.45 was obtained at 573 K. The actual thermal conductivity at this temperature was smaller than at 298 K. Therefore, the value is larger than the zT value of 2.45, and the

application of this material in the medium-to-high temperature range is feasible.

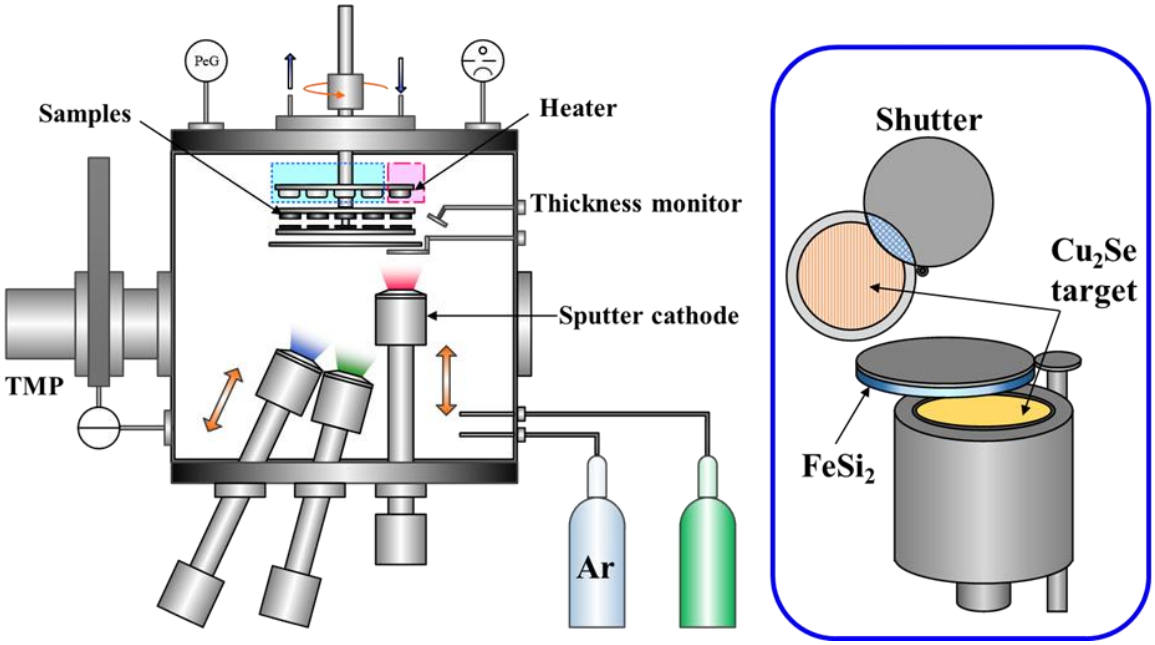

Figure S1 Schematic of the combinatorial sputter coating system.

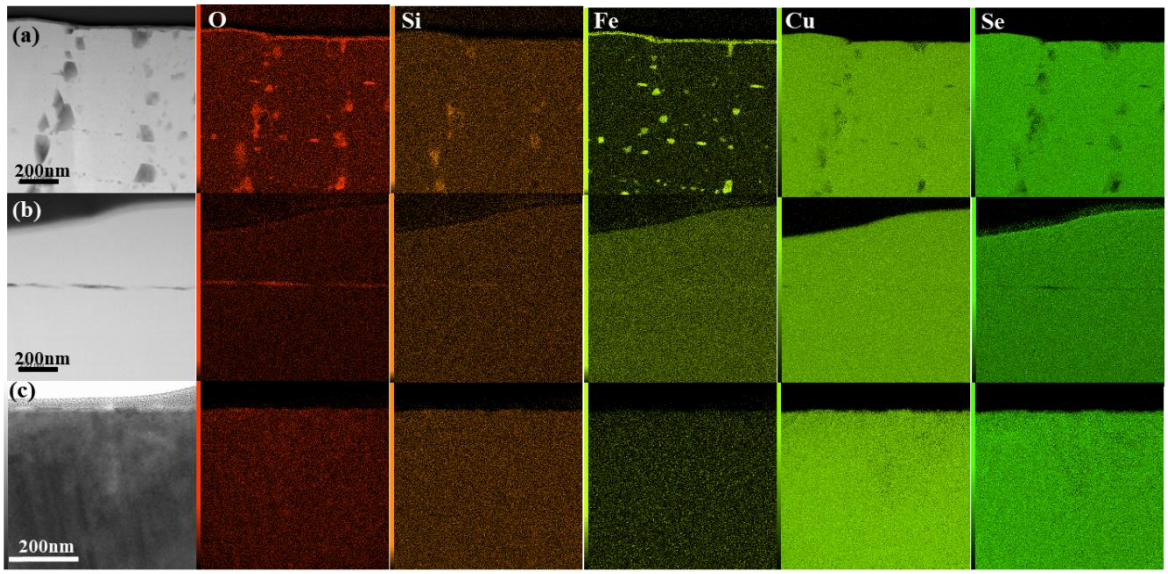

Figure S2 Energy-dispersive X-ray spectroscopy elemental maps of CSSFO thin films under varying coating conditions: 60 W, 298 K (a); 60 W, 773 K (b); and 120 W, 773 K (c).

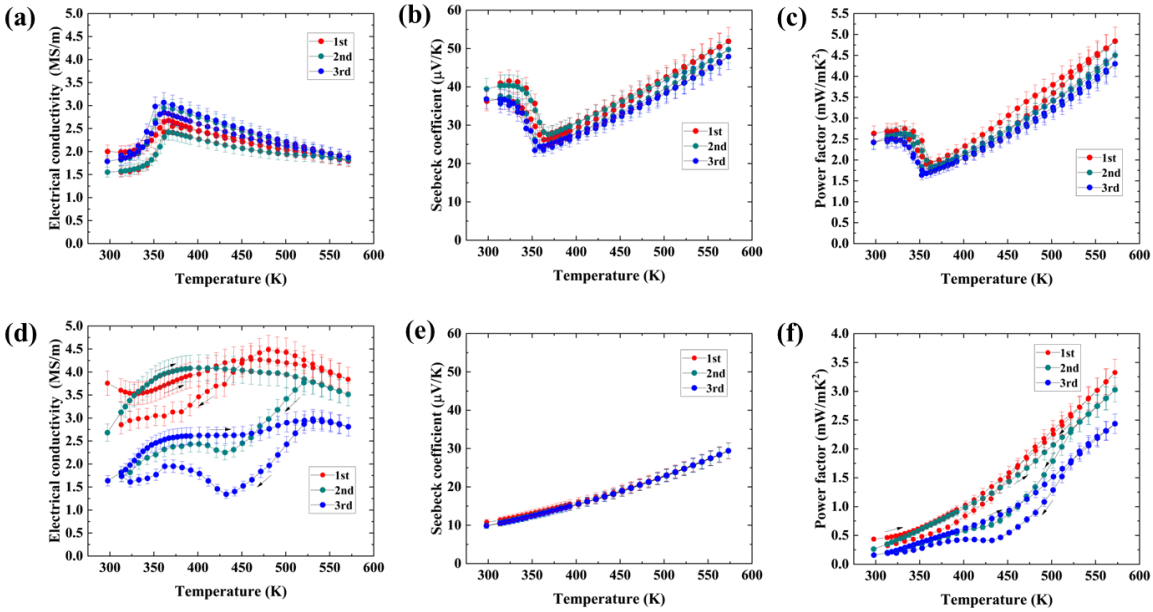

Figure S3 Thermoelectric properties of CSSFO thin films measured over three repeated cycles: 120 W, 773 K (a–c) and 60 W, 298 K (d–f).

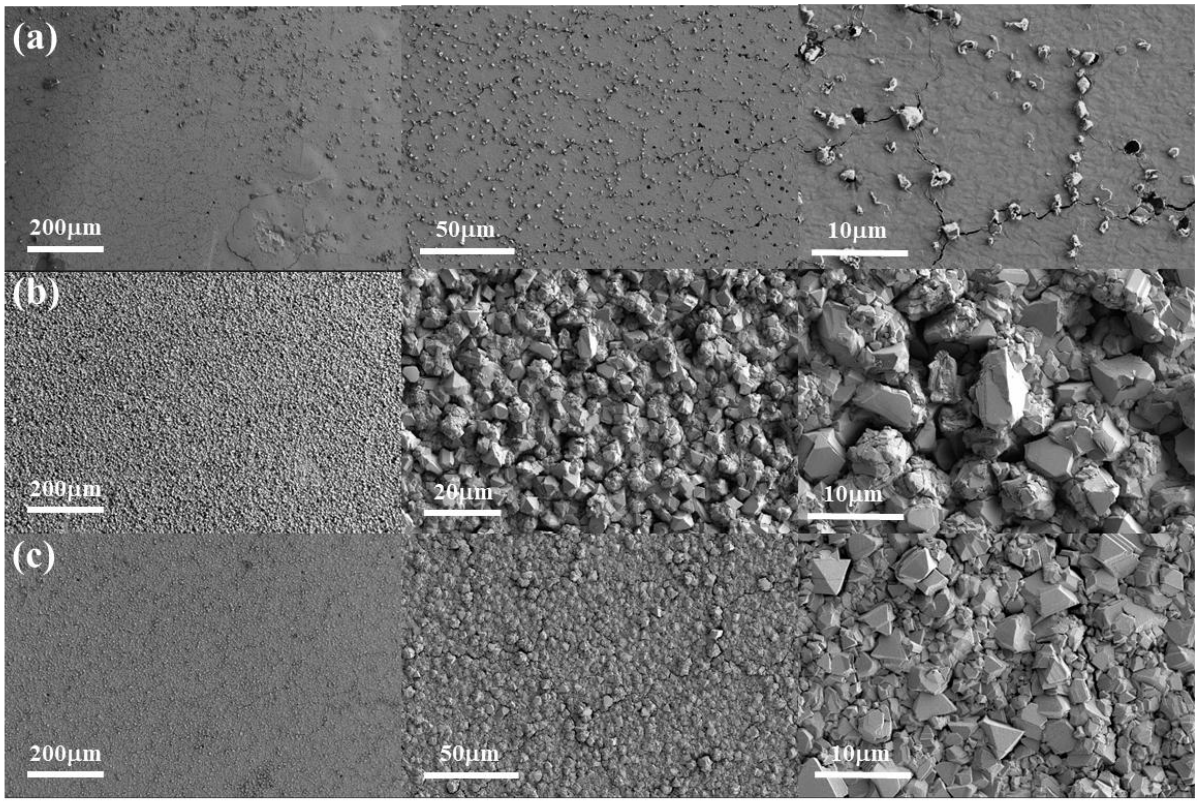

Figure S4 Scanning electron microscopic images of CSSFO thin films under varying coating conditions: 60 W, 298 K (a); 60 W, 773 K (b); and 120 W, 773 K (c).

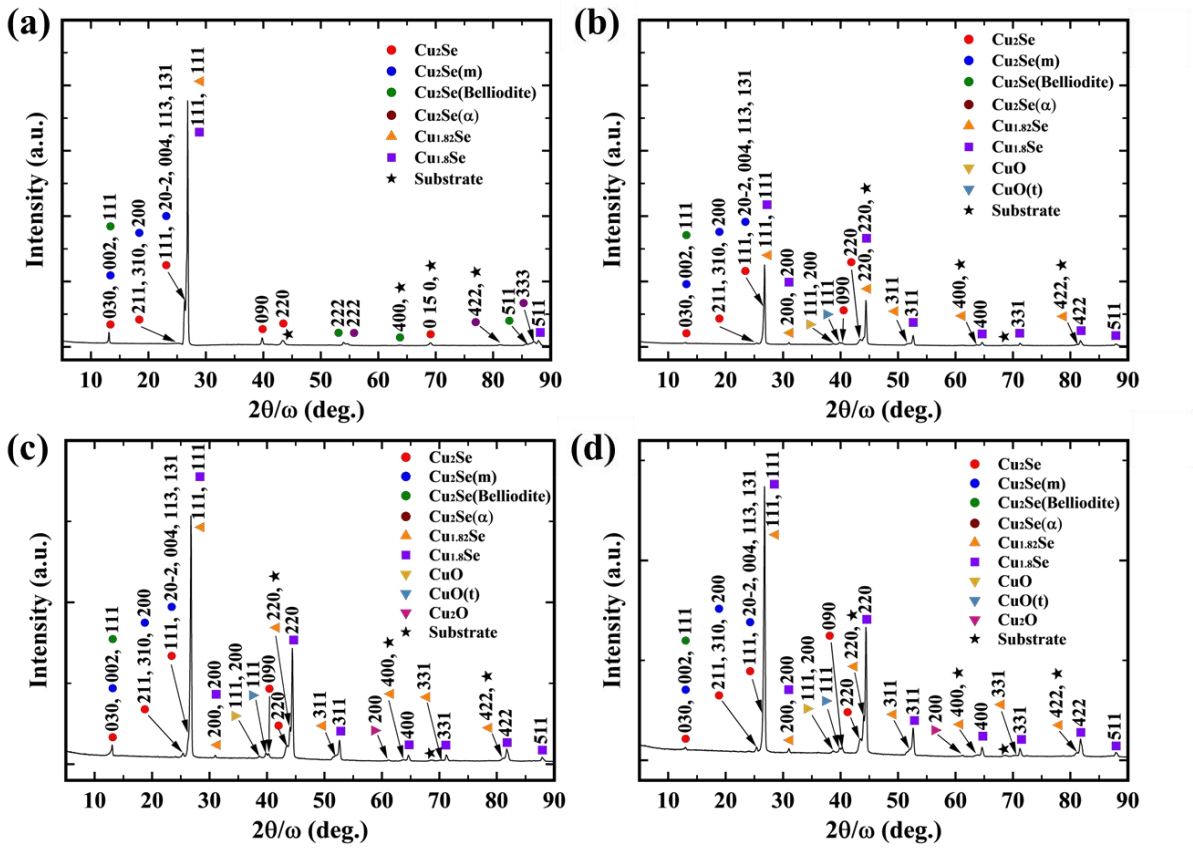

Figure S5 X-ray diffraction spectra of CSSFO thin films under varying coating conditions: 60 W, 298 K (a); 60 W, 773 K (b); 80 W, 773 K (c); and 100 W, 773 K (d).

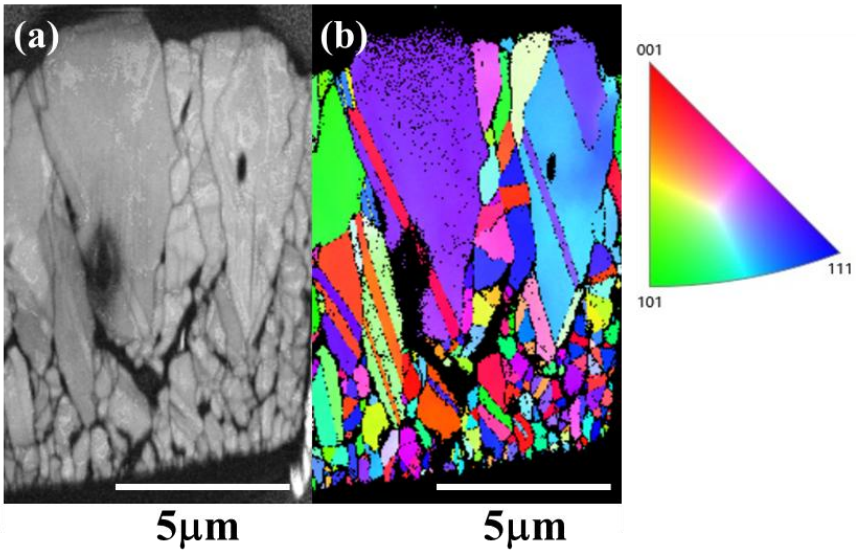

Figure S6 Electron backscattered diffraction images of a CSSFO thin film prepared at 120 W and 773 K. Band contrast (a). Inverse pole figure map (b). The film exhibits various crystal structures and preferred crystal orientations. The crystal grain size was smaller near the substrate, and it increased progressively toward the surface.

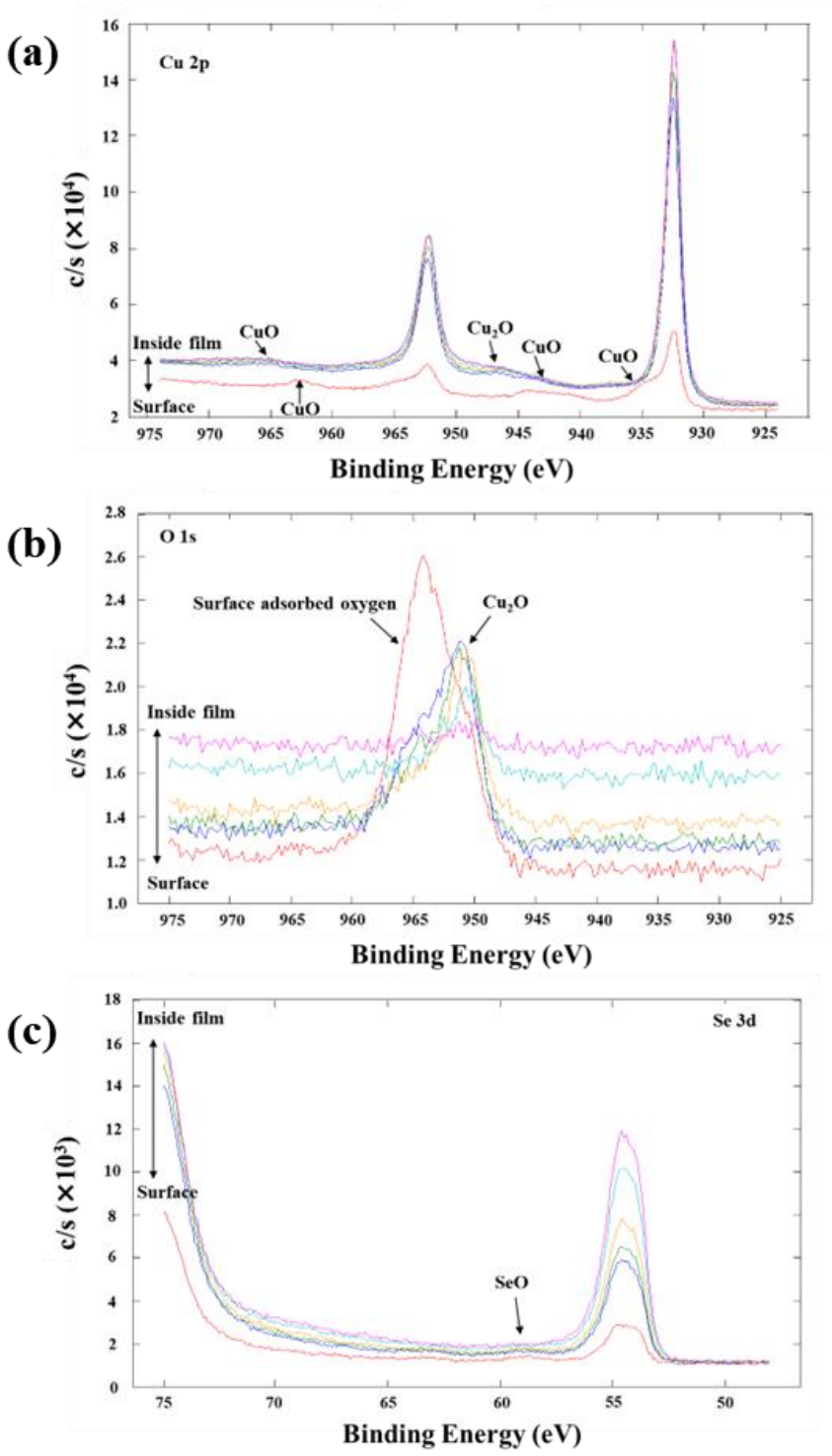

Figure S7 X-ray photoelectron spectroscopy of the CSSFO thin film prepared at 120 W and 773 K: Cu 2p peak (a), O 1s peak (b), and Se 3d peak (c).

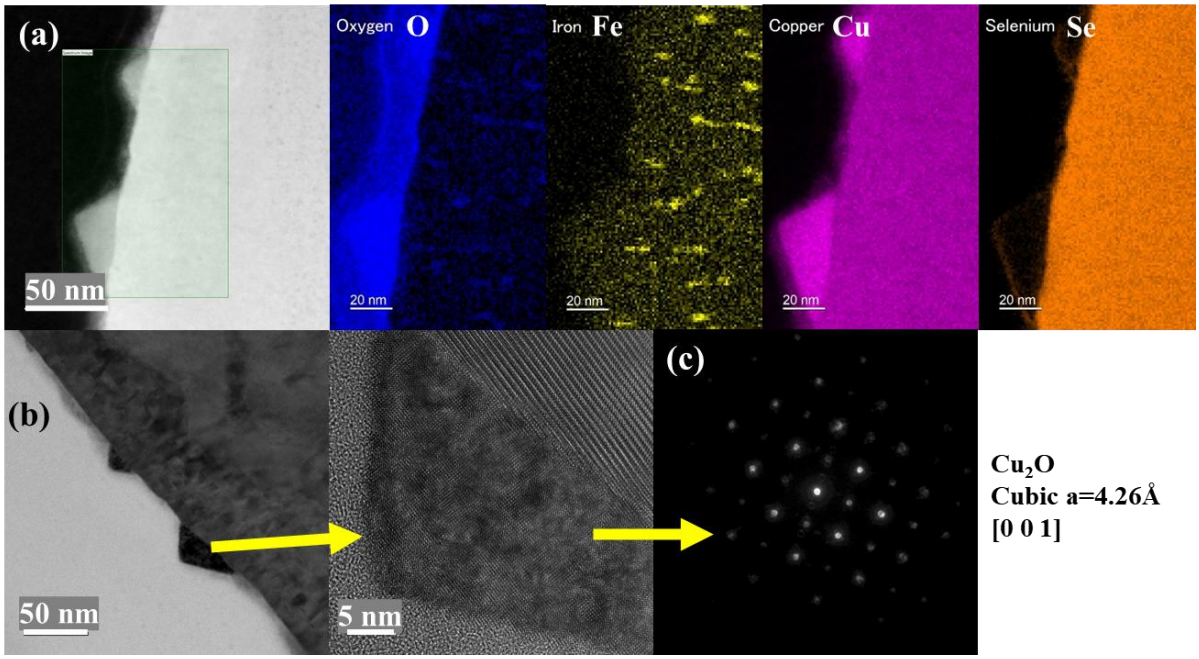

Figure S8 Elemental mapping and electron diffraction images of the tetrahedron-like structures on the surface of CSSFO thin films prepared at 120 W and 773 K. Based on the elemental mapping, the structures consist of Cu, O, and small amounts of Fe (a). High-resolution transmission electron microscopic image showing the crystalline nature of the structures (b). Electron diffraction analysis confirms that the crystal structure corresponds to Cu_2O (c).

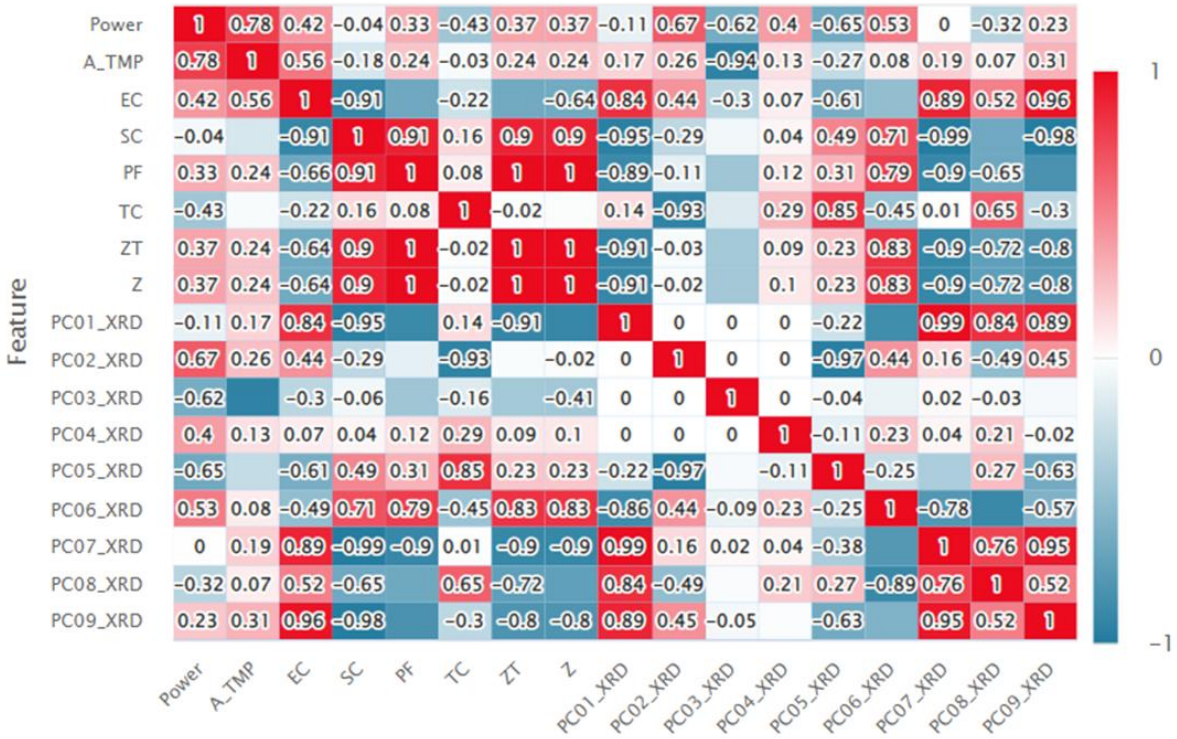

Figure S9 Heatmap of Lasso analysis. The contribution ratio of each component was 90% for PC1 and 9% for PC2, and these two components are the main factors. Reducing PC1 and PC2 can effectively improve the zT value.

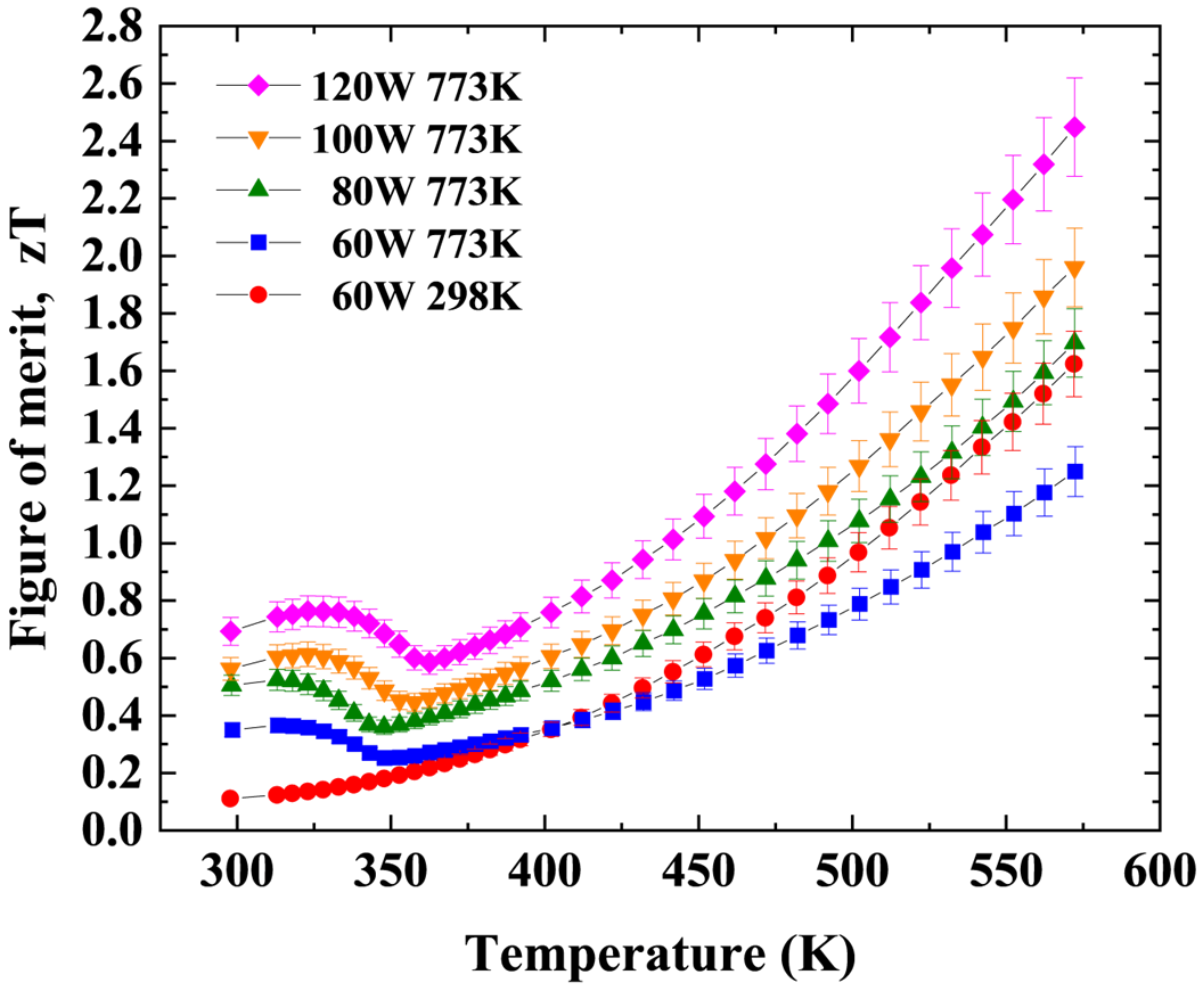

Figure S10 Temperature dependence of the zT value of $Cu_2Se_xSi_yFe_zO_t$ films with the radiofrequency (RF) power and substrate temperature.